AIAA JOURNAL
Vol. 45, No. 11, November 2007

Efficient Approach for Multipoint Aerodynamic Wing Design of Business Jet Aircraft

Boris Epstein*
Academic College of Tel-Aviv-Yaffo, 64044 Tel-Aviv, Israel
and
Sergey Peigin†
Israel Aircraft Industries, 70100 Ben-Gurion Airport, Israel

DOI: 10.2514/1.29307

An efficient computational-fluid-dynamics-driven approach to multipoint constrained aerodynamic wing design for business jet aircraft is proposed. This method significantly extends the capabilities of the optimization tool OPTIMAS, previously developed by the authors, for aerodynamic design of three-dimensional isolated wings. In the framework of the method, the total drag of an optimized aircraft configuration is minimized at fixed lift values subject to numerous geometrical and aerodynamical constraints. The optimum search is driven by genetic algorithms and is based on full Navier–Stokes computations supported by massive multilevel parallelization. The applications include a series of single- and multipoint aerodynamic design optimizations for a generic business jet. For the considered class of shape optimizations, significant drag reduction in on- and off-design conditions has been achieved.

I. Introduction

THE growing competitiveness in aircraft industry calls for an accurate, efficient, and robust tool for advanced aerodynamic shape design. The main goal of such a tool is to produce a configuration suited to the aircraft mission with the lowest possible flight costs.

In this connection, to additionally underline the importance of drag minimization, consider the task of delivering a payload between distant destinations. The Breguet range equation [1], which applies to long-range missions of jet-aircraft, implies [2] that the operator would have to reduce the payload (and thus reduce the revenue) by 7.6% to recover the 1.0% increase in drag. Because most airlines operate on small margins, this service would most likely no longer be a profit-generating venture. This illustrates that a 1% delta in total drag is a significant change.

In the development of commercial aircraft, aerodynamic design plays a leading role during the preliminary design stage, when the external aerodynamic shape is typically finalized. This phase is estimated by a cost of 60–120 million dollars [2]. The final design would be normally carried out only upon the commercially promising completion of the preliminary stage, which makes the preliminary design stage crucial for the overall success of the project.

Because of the importance of this stage (for which, according to [2], a staff of 100–300 people is generally employed for up to two years), let us go into detail. The aerodynamic design process is embedded in the overall preliminary design, with the starting point coming from the conceptual design. The inner loop of aerodynamic analysis is included into an outer (multidisciplinary) loop that is a part of a major design cycle. Because of the limitations of the overall design technology, this cycle is usually repeated a number of times. For example, in recent Boeing practice, three major design cycles, each requiring 4–6 months, have been used to finalize the wing design [2]. Thus, the introduction of a computational-fluid-dynamics (CFD)-driven robust automatic aerodynamic optimization, which will allow us to reduce the number of design cycles, would significantly shorten the overall design process.

The past three decades brought a revolution in the entire process of aerodynamic design, due to the increasing role of computational simulation. In the beginning, the applicability of CFD to the aerodynamic design was confined to flow analysis in a limited range of flight conditions and aerodynamic shapes. Additional limitations were due to the variable accuracy level in prediction of different aerodynamic characteristics.

Over the years, CFD-driven optimization methods appeared [2–13]. Though the subject has aroused considerable interest in many researchers and aircraft companies, the practical impact of available optimization techniques is, to the best of our knowledge, rather limited from the industrial viewpoint.

In this context, the main goal of this paper is to present an accurate and computationally efficient approach to the multipoint constrained aerodynamic wing design for business jet aircraft. This method significantly extends the capabilities of the optimization tool OPTIMAS, previously developed by the authors, for aerodynamic design of 3D isolated wings [14]. In the framework of the method, the total drag of an optimized aircraft configuration is minimized at fixed lift values subject to numerous geometrical and aerodynamical constraints. The optimum search is driven by genetic algorithms and is based on full Navier–Stokes drag prediction, supported by massive multilevel parallelization of the whole computational framework.

The applications include a series of single- and multipoint aerodynamic optimizations for a generic business jet. It was demonstrated that the proposed method allows us to design feasible aerodynamic shapes that possess a low drag at cruise conditions, satisfy a large number of geometrical and aerodynamic constraints, and offer a good off-design performance in markedly different flight conditions such as takeoff and high-Mach zone.

II. Statement of the Problem

The input parameters of the aerodynamic configuration design include prescribed cruise lift, Mach, altitude, and minimum allowed drag values, which should ensure the aerodynamic goals of the aircraft mission (such as range, payload, fuel volume, etc.). The desired geometry is sought in the class of solutions that satisfy different geometrical, aerodynamic, and multidisciplinary constraints.

The design goal is to develop a geometry with as low a drag at cruise conditions as possible and that, at the same time, satisfies the preceding constraints.

Received 14 December 2006; revision received 27 June 2007; accepted for publication 1 August 2007.

*Professor, Computer Sciences Department, 4 Antokolsky Street. Member AIAA.
†Professor, Engineering Division. Senior Member AIAA.

The main idea behind the proposed approach is to accomplish this objective through a CFD-based solution of the properly formulated multipoint constrained optimization problem.

The set of constraints may be divided into the following two classes: the class of geometrical constraints and the class of aerodynamic constraints. The geometrical constraints are mostly independent of flight conditions and are easily verified, whereas aerodynamic constraints naturally depend on flight conditions and necessitate heavy CFD runs for their verification.

Concerning the choice of the objective function, it is assumed that the drag coefficient C_D of a tested configuration is a sensitive and reliable indicator of its aerodynamic performance, and thus we employ C_D as the objective function of the considered optimization problem.

Another crucial issue is the implementation of constraints in the framework of the optimization algorithm. When possible, the constraints should be satisfied exactly in the direct way, whereas the remaining constraints should be converted into alternative constraints that can be expressed in terms of drag. For example, in the proposed approach, the geometrical constraints and such aerodynamic constraints as the prescribed lift coefficient are satisfied exactly, whereas the requirement of a sufficiently high $C_L^{\max}$ at the takeoff conditions is reformulated in terms of drag at the corresponding flight conditions.

Finally, to ensure the accuracy of optimization, we require that for any geometry feasible from the constraints' viewpoint, the value of the objective (cost) function remains exactly equal to the value of the drag coefficient without any penalization.

Based on the preceding ideas, the mathematical formulation of the optimization problem for which the solution allows us to achieve the design goal may be expressed as follows.

The objective of the general multipoint optimization problem is to minimize the weighted combination C_D^{wtd} of drag coefficients at the main design and secondary design points (flight conditions):

$$C_D^{\text{wtd}} = \sum_{k=1}^{K} w_k C_D(k)$$

where K is the total number of design points.

The solution is sought in the class of wing shapes subject to the following classes of constraints:

1) Aerodynamic constraints such as prescribed constant total lift coefficient $C_L^*(k)$ and maximum allowed pitching moment $C_M^*(k)$:

$$C_L(k) = C_L^*(k), \qquad C_M(k) \geq C_M^*(k) \tag{1}$$

2) Geometrical constraints on the shape of the wing surface in terms of properties of sectional airfoils at the prescribed wing span locations: relative thickness $(t/c)_i$, relative local thickness $(\Delta y/c)_{ij}$ at the given chord locations $(x/c)_{ij}$ (beam constraints), relative radius of leading edge $(R/c)_i$, and trailing-edge angle θ_i:

$$\begin{gathered}(t/c)_i \geq (t/c)_i^*, \qquad (\Delta y/c)_{ij} \geq (\Delta y/c)_{ij}^* \\ (R/c)_i \geq (R/c)_i^*, \qquad \theta_i \geq \theta_i^* \qquad i = 1, \ldots, N_{\text{ws}} \\ j = 1, \ldots, N_{\text{bc}}(i)\end{gathered} \tag{2}$$

where N_{ws} is the total number of sectional airfoils subject to optimization; $N_{\text{bc}}(i)$ is the total number of beams constraints at section i; and values $(t/c)_i^*$, $(\Delta y/c)_{ij}^*$, θ_i^*, $(R/c)_i^*$, C_L^*, and C_M^* are prescribed parameters of the problem.

Thus, in the present work, the total number of considered constraints N_{cs} is equal to

$$N_{\text{cs}} = 2 \times K + 3 \times N_{\text{ws}} + \sum_{i=1}^{N_{\text{ws}}} N_{\text{bc}}(i)$$

In principle, the present optimization method allows for handling a large number of constraints of different natures in addition to the preceding descriptions.

As a gas-dynamic model for calculating C_D, C_L, and C_M values, the full Navier–Stokes equations are used. Numerical solution of the full Navier–Stokes equations was provided by the multiblock code NES [15], which employs structured point-to-point matched grids. The code is based on the essentially nonoscillatory concept with a flux interpolation technique [16], which allows for accurate estimation of sensitive aerodynamic characteristics such as lift, pressure drag, friction drag, and pitching moment.

The code ensures high accuracy of the Navier–Stokes computations and high robustness for a wide range of flows and geometrical configurations. The high performance of NES was systematically demonstrated by testing it in a wide range of aerodynamic configurations of different complexity: from one-element 2D airfoils through transport-type supercritical wings and ARA M100 wing–body geometry [15] to wing–body nacelle-pylon DLR-F6 aircraft configuration [17].

The important advantage of the solver NES as a driver of optimization process is its ability to provide reliable and sufficiently accurate results already on relatively coarse meshes and thus to dramatically reduce the volume of CFD computations.

III. Optimization Algorithm

In this section, we briefly describe the optimization method recently developed by the authors. Two-dimensional applications of the method may be found in [18], and the optimization of isolated 3D wings was considered in [14].

The driver of the optimization search is a variant of genetic algorithms (GAs). The main features of the method include a new strategy for efficient handling of nonlinear constraints in the framework of GAs, scanning of the optimization search space by a combination of full Navier–Stokes computations with the reduced-order models method, and multilevel parallelization of the whole computational framework, which efficiently makes use of computational power supplied by massively parallel processors.

A. Parameterization of the Search Space

The choice of an appropriate search space is of crucial importance for the whole optimization algorithm. The search space should include a wide spectrum of shapes to be sufficiently representative and, at the same time, the total number of parameters should not be too high (to ensure a successful and efficient search).

For the considered class of optimization problems, this problem may be satisfactory resolved. The point is that in the case of wing–body optimization for minimum drag, the main object of optimization is the lifting surface of the aircraft. Thus, the whole surface of the aircraft may be divided into two parts. The first part of the surface (which contains all the points located on the aircraft fuselage) does not change in the course of optimization process and thus does not necessitate any parameterization.

In our case, the object of optimization is the second part of the surface, which contains all the points located on the wing and thus requires the parameterization. For this specific class of 3D aerodynamic lifting surfaces (such as a wing in wing–body configurations), the global geometrical representation of the whole shape from the root section up to the tip region is available.

In this work, the following is assumed:

1) The geometry is described by the absolute Cartesian coordinate system (x, y, z), where the axes x, y and z are directed along the streamwise, normal to the wing surface, and spanwise directions, respectively.

2) The wing projection on the plane (x, z) (wing planform) is fixed.

3) The wing surface is generated by a linear interpolation (in the spanwise direction) between sectional 2D airfoils.

4) The number of sectional airfoils N_{ws} is fixed.

5) The wing–body boundary (the wing root airfoil) is not subject to change in the optimization process.

6) The shape of the sectional airfoils is determined by Bezier splines. In the absolute coordinate system, the location of the preceding profiles is defined by the corresponding span positions of

the trailing edge on the wing planform, twist angles $\{\alpha_i^{\text{tw}}\}$, and dihedral values $\{\gamma_i^{\text{dh}}\}$ (relative to the root section).

The current version of the optimization tool OPTIMAS deals with a fixed-wing planform that comes from the conceptual design stage and it is determined by structural considerations.

The wing planform is defined by the following preset parameters: the chord length at the root section c_1, the span location of the wing sections $\{z_i\}$, and the corresponding leading and trailing-edge sweep angles ($\{\lambda_i^{\text{le}}\}$ and $\{\lambda_i^{\text{tr}}\}$).

For each wing section, the nondimensional shape of the airfoil (scaled by the corresponding chord) is defined in a local Cartesian coordinate system $(\bar{x}, \bar{y})$ in the following way. The coordinates of the leading edge and trailing edge of the profile were, respectively, (0, 0) and (1, 0). For an approximation of the upper and lower airfoil surface, Bezier spline representation was used. A Bezier curve of order N is defined by the Bernstein polynomials $B_{N,i}$ (C_N^i binomial coefficients):

$$\boldsymbol{G}^k(t) = \sum_{i=0}^{N} B_{N,i}\boldsymbol{P}_i^k, \qquad B_{N,i} = C_N^i t^i (1-t)^{N-i}$$
$$C_N^i = \frac{N!}{i!(N-i)!} \tag{3}$$

where t denotes the curve parameter taking values in [0, 1], $\boldsymbol{P}_i^k$ are the control points, and superscript $k = u, l$ corresponds to the upper and lower surfaces of the profile. So, as seen from Eq. (3), the Bezier curve is completely determined by the Cartesian coordinates of the control points.

For the considered optimization problem, the first $\boldsymbol{P}_0^k = (0, 0)$ and the last $\boldsymbol{P}_N^k = (1, 0)$ ($k = u, l$) points are set just fixing the position of leading and trailing edges. We also fix all the abscissas x_i^k of the control points $\boldsymbol{P}_1^k, \ldots, \boldsymbol{P}_{N-1}^k$. We set $x_1^k = 0$ to ensure that the upper and lower surfaces of the profile are tangent to the y axes at the leading edge. Finally, assuming the continuity of the airfoil curvature at the leading edge we obtain the additional relation $y_1^u = -y_1^l$.

Thus, the shape of a sectional profile is completely determined by a total of $2N - 5$ parameters $(a_1, a_2, \ldots, a_{N-1}, a_N, \ldots, a_{2N-5})$:

$$a_j = y_j^u, \qquad 1 \le j \le (N-1)$$
$$a_j = y_{j-N+2}^l, \quad N \le j \le (2N-5)$$

To fully specify the wing shape, it is necessary to set locations of the 2D sectional airfoils, in addition to their shapes. Assuming that the chord value and trailing-edge location are defined by the wing planform, the sectional locations are specified by means of two additional design variables per section: twist angle $\{\alpha_i^{\text{tw}}\}$ and dihedral value $\{\gamma_i^{\text{dh}}\}$. Note that for the root section, these values are set to zero.

Thus, the design variables include $2N - 5$ Bezier coefficients and twist and dihedral values (for each design wing section), and the dimensions N_D of the search space are equal to

$$N_D = (N_{\text{ws}} - 1) \cdot (2N - 3)$$

Finally, the search string S contains N_D floating-point variables a_j ($j = 1, \ldots, N_D$). The string components are varied within the search domain D. The domain D is determined by values $\min_j$ and $\max_j$, which are the lower and upper bounds of the variable a_j.

B. Search Algorithm

As a basic search algorithm, a variant of the floating-point GA [19] is used. The mating pool is formed through the use of tournament selection. This allows for an essential increase in the diversity of the parents. We employ the arithmetical crossover and the nonuniform real-coded mutation defined by Michalewicz [19]. To avoid a premature convergence of GA, we applied the mutation operator in a distance-dependent form [20]. To improve the convergence of the algorithm, we also use the elitism principle.

In the considered optimization problem, the presence of constraints has a great impact on the solution. This is due to the fact that the optimal solution does not represent a local minimum in the conventional sense of the word. Instead, it is located on an intersection of hypersurfaces of different dimensions, generated by linear and nonlinear constraints. Additionally, the problem of finding such an extremum is essentially complicated by the fact that these hypersurfaces, which bound the feasible search space, are not known in advance and may possess irregular topology.

For example, it is aerodynamically expected that in the case of the thickness-constrained optimization, the optimal wing should possess the minimum allowed thickness. This implies that the optimal point should reside exactly on the corresponding hypersurface.

In the case of constraints imposed on the aerodynamic characteristics such as pitching moment C_M, the situation is even less controlled. Similar to the previous example, the optimal solution should be located exactly on the constraint boundary. But contrary to the case of geometrical constraints, the determination of the boundary is a much heavier computational problem. For the geometrical constraints, the feasibility test is computationally very cheap, whereas in the case of aerodynamic constraints, the corresponding test requires a full (computationally heavy) CFD run.

In their basic form, genetic algorithms are not capable of handling constraint functions limiting the set of feasible solutions. To resolve this, a new approach has been proposed that can be basically outlined as follows (for more detail, see [21]):

1) Instead of the traditional approach in which only feasible points may be included in a path, it is proposed to employ search paths through both feasible and infeasible points.

2) With this end in view, the search space is extended by evaluating (in terms of fitness) the points, which do not satisfy the constraints imposed by the optimization problem. A needed extension of an objective function may be implemented by means of GAs, due to their basic property; contrary to classical optimization methods, GAs are not confined to only smooth extensions.

Based on this approach to the constraint handling, the modified objective function Q was defined as follows:

$$Q = \begin{cases} 0.1 + [(t/c)_i^* - (t/c)_i] & \text{if } (t/c)_i < (t/c)_i^* \\ 0.125 + [(\Delta y/c)_{ij}^* - (\Delta y/c)_{ij}] & \text{if } (\Delta y/c)_{ij} < (\Delta y/c)_{ij}^* \\ 0.15 + [C_M^* - C_M] & \text{if } C_M < C_M^* \\ 0.2 + [R_i^* - R_i] & \text{if } R_i < R_i^* \\ 0.3 + [\theta_i^* - \theta_i] & \text{if } \theta_i < \theta_i^* \\ 0.5 & \text{if } y_i^u(t) < y_i^l(t) \\ C_D & \text{otherwise} \end{cases} \tag{4}$$

where each condition is tested independently for all i and j [$(i = 1, \ldots, N_{\text{ws}},\ j = 1, \ldots, N_{\text{bc}}(i)$]. In the case of multipoint optimization, the value of C_D represents a weighted combination of total drag values at the flight points participating in optimization. The specific values of the relative weights are chosen in the way that roughly ensures the equal contribution of each flight point in the modified objective function.

C. Approximation of Objective Function

Low computational efficiency of GAs is the main obstacle to their practical use when the evaluation of the cost function is computationally expensive, as happens in the framework of the full Navier–Stokes model.

A simple estimation demonstrates that even for a moderate population size of $M = 100$, at least 20,000 evaluations of the cost function (CFD solutions) are required to reach the appropriate convergence. A fast full Navier–Stokes evaluation over a 3D wing–body aircraft configuration takes at least 30–40 min of CPU time. Consequently, the direct use of such an algorithm is practically unacceptable.

To resolve this problem, we employ an intermediate "computational agent": a computational tool that, on one hand, is based on a very limited number of exact evaluations of objective function and, on the other hand, provides a fast and reasonably accurate computational feedback in the framework of GA search.

In this work, we use the reduced-order model approach, in which the solution functionals are approximated by a local database. The database is obtained by solving the full Navier–Stokes equations in a discrete neighborhood of a basic point (basic geometry) positioned in the search space. Specifically, a mixed linear-quadratic approximation is employed. One-dimensionally, the one-sided linear approximation is used in the case of monotonic behavior of the approximated function, and the quadratic approximation is used otherwise.

To ensure the accuracy and robustness of the method, a multidomain prediction-verification principle is employed. That is, at the prediction stage, the genetic optimum search is concurrently performed on a number of embedded search domains. As a result, each domain produces an optimal point, and the whole set of these points is verified (through full Navier–Stokes computations) at the verification stage of the method, and thus the final optimal point is determined. It is important to note that the Navier–Stokes computations are actually performed only for the database construction ($2N_D$ computations) and for the verification of optimal points (the number of computations is equal to the number of search domains). More details can be found in [18].

In addition, to ensure the global character of the search, it is necessary to overcome the local nature of the preceding approximation. For this purpose, it is suggested to perform iterations in such a way that in each iteration, the result of optimization serves as the initial point for the next iteration step (further referred to as the optimization step).

D. Automatic Grid Transformation

In the present context, each CFD run requires a different geometry and, therefore, the construction of a new computational grid. For novel complex geometries, meshes are generally constructed manually, which is very time-consuming and prohibitive in the framework of a automatic optimization tool.

The needed continuity of optimization stream is maintained by using topological similarity of geometrical configurations involved in the optimization process. The required grids are constructed by means of a fast automatic transformation of the initial grid, which corresponds to the starting basic geometry.

The preceding fast transformation of grids was implemented in the following way. First, the wing–body configuration surface was divided into four parts. The first part comprises the fuselage surface points and the second part (inner wing) includes the surface points lying in the region $z_{\text{root}} + \Delta z_{\text{root}} \le z \le z_{\text{tip}}$. The last two parts are the tip region ($z > z_{\text{tip}}$) and the root region ($z_{\text{root}} < z < z_{\text{root}} + \Delta z_{\text{root}}$), where z_{root} and z_{tip} are the span locations of the root and tip wing sections, respectively.

The transformation of the surface includes three stages. Assume that the grid possesses i, j, and k structure, with the coordinate plane $j = 0$ representing the grid points lying on the configuration surface; $\Delta\mathbf{r}_{i,0,k}$ denote the change in the geometry of the surface at a grid point with indices $(i, 0, k)$. For the inner part of the wing (the second part), $\Delta\mathbf{r}_{i,0,k}$ represent the differences between the current geometry and the basic grid. For the tip and the root regions (the third and the fourth parts), $\Delta\mathbf{r}_{i,0,k}$ are determined in a way that ensures a smooth conjugation of these parts with the inner wing region and fuselage region. For the first part of the surface partition (the fuselage region), the corresponding $\Delta\mathbf{r}_{i,0,k}$ values are set to zero.

At the first stage, the coordinates $\mathbf{r}^{\text{new}}_{i,j,k}$ of the new grid are obtained by propagation of the shift $\Delta\mathbf{r}_{i,0,k}$ along the grid line $i = \text{const}$ and $k = \text{const}$:

$$\mathbf{r}^{\text{new}}_{i,j,k} = \mathbf{r}^{\text{initial}}_{i,j,k} + \Delta\mathbf{r}_{i,0,k}$$

At the second stage, the twist transformation is performed. For each grid point, the z coordinate is fixed, whereas the x and y coordinates are modified in accordance with the value of the twist angle obtained by the linear interpolation from the nearby wing sections.

Finally, the dihedral transformation is applied. Here, x and z coordinates are fixed, whereas the y coordinate is shifted in accordance with the interpolated value of dihedral.

E. Parallelization of the Optimization Stream

The problem of optimization of aerodynamic shapes is very time-consuming because it requires a huge amount of computational work. Each optimization step requires a number of heavy CFD runs, and a large number of such steps is needed to reach an optimum. Thus, the construction of a computationally efficient algorithm is vital for the success of the method in engineering environment.

To reach this goal, it was proposed to employ an embedded multilevel parallelization strategy [22]: Level 1 is parallelization of the full Navier–Stokes solver. Level 2 is parallel CFD scanning of the search space. Level 3 is parallelization of the GA optimization process. Level 4 is parallel optimal search on multiple search domains. Level 5 is parallel grid generation.

The first parallelization level (for a detailed description see [23]) is based on the geometrical decomposition principle. All processors are divided into two groups: one master processor and N_s slave processors. A large body of computational data demonstrated that the preceding approach for parallel implementation of the multiblock full Navier–Stokes solver enables one to achieve a high level of parallel efficiency while retaining high accuracy of calculations and thus to significantly reduce the execution time for large-scale CFD computations.

The first level of parallelization is embedded with the second level, which performs parallel scanning of the search space and thus provides parallel CFD estimation of fitness function on multiple geometries.

The third level parallelizes the GA optimization work unit. At this level of parallelization, all the processors are divided into one master processor and P_s slave processors. The goal of the master processor is to distribute the initial random populations among the slaves and to get back the results of optimal search (P_s is the number of initial random populations).

The third level of parallelization is embedded with the fourth level, which performs parallel optimal search on multiple search domains. At this level of parallelization, all the processors are divided into three groups: one main processor, P_m master processors, and $P_m \cdot P_s$ of slave processors (where P_m is equal to the number of domains).

The fifth parallelization level handles the grid generation process. At this level, one master processor and G_s slave processors are employed (G_s is the number of evaluated geometries).

Finally, we can conclude that the five-level parallelization approach allowed us to sustain a high level of parallel efficiency on massively parallel machines and thus to dramatically improve the computational efficiency of the optimization algorithm.

IV. Analysis of Results

The method was applied to the problem of multipoint, multiconstrained, transonic wing optimization for a generic business jet aircraft. The configuration includes a realistic fuselage and a cranked glovelike high-aspect-ratio wing.

The CFD solver NES (used as a driver of the optimization process) ensures high accuracy of the Navier–Stokes computations on relatively coarse grids, as well as robustness for a wide range of flows and geometrical configurations. High performance of NES was systematically demonstrated by testing it in a wide range of aerodynamic configurations of different complexity: from one-element 2D airfoils through transport-type supercritical wings up to full wing–body configurations [15,17,24]. The results by the code NES demonstrated a high accuracy of drag prediction (within several counts) in the whole range of flight conditions. Note that the prediction accuracy of component drag increments (with the naelle on and off) was even higher. This is indicative of the NES suitability as a CFD driver of the optimization process.

For transonic wing–body configurations, NES provides accurate asymptotically converged estimates of aerodynamic coefficients, with C-O topology grids containing, on the fine level, about 325

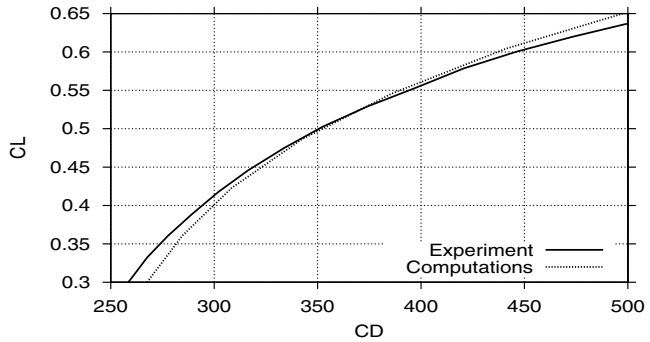

Fig. 1 Generic business jet wing–body; drag polars at $M = 0.80$; numerical computations vs experimental data.

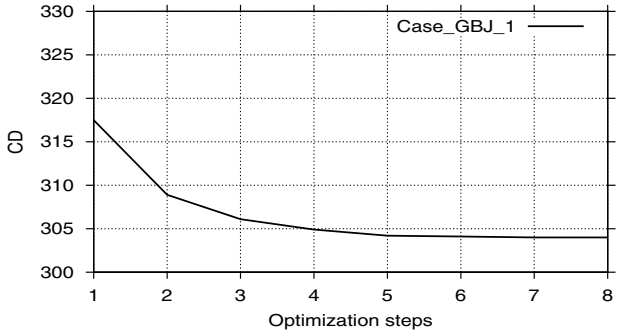

Fig. 2 Generic business jet wing–body; convergence history for case GBJ 1.

points around the configuration, 57 points normal to the surface, and 49 points in the spanwise direction. Specifically, for the considered generic business jet wing–body shape, the code NES was verified through systematic comparison with experimental data. An example of the comparison is given in Fig. 1, in which the drag polars at $M = 0.80$ are presented.

The following example deals with the verification of the optimization method by itself. In this test case, the optimization of a classical ONERA M6 wing in transonic conditions was considered.

This wing was employed as a 3D optimization test case by a number of authors. In this work, the comparison with results presented by Weinerfelt [25] was carried out. In [25], the CFD driver was an Euler solver and the optimizer was gradient-based.

In this connection, to allow for a consistent comparison, we performed the optimization at the design point $C_L = 0.3$ ($M = 0.84$) by means of the Euler CFD driver. We use the same constraints (flow and geometry) that were employed in [25]. The set of computational grids contained three multigrid levels. Each level included eight blocks. The total number of points in the fine level was close to 200,000.

The results of comparison are as follows. In [25] (Euler CFD driver), an initial pressure drag of 153 aerodynamic counts was reduced by 34 counts to a level of 119 counts. In the present Euler-driven optimization, the reduction of pressure drag was equal to 53 counts (from the original 148.1 counts to 95.1 counts).

We may conclude that although the drag values estimated by the preceding codes for the initial ONERA M6 configuration are close to one another, the drag reduction by the present method is significantly higher.

In the following, we present the results of one- and multipoint drag minimization for a generic business jet aircraft. The geometrical constraints (per section) were placed upon relative maximum thickness, local relative leading-edge radius (the radius of curvature of a nondimensional wing section at $\bar{x} = 0$) and trailing-edge angle (measured at $\bar{x} = 1$), and relative local thickness at two fixed x/c locations (beam constraints). An additional (aerodynamic) constraint was imposed on the value of pitching moment. In all the considered test-cases, the values of all the preceding geometrical constraints were kept to the level of the original geometry.

Table 1 Generic business jet wing–body configuration; optimization conditions and constraints

Case no.	C_L^*	M	w_i	C_M^*	$N_{bc}(i)$
Case GBJ 1	0.52	0.75	1.0	$-\infty$	0
Case GBJ 2	0.40	0.80	1.0	$-\infty$	0
Case GBJ 3	0.40	0.80	1.0	$-\infty$	2
Case GBJ 4	0.40	0.80	1.0	−0.136	0
Case GBJ 5	0.40	0.80	1.0	−0.136	2
Case GBJ 6	0.40	0.80	0.95	−0.136	2
	1.50	0.20	0.05	$-\infty$	2
Case GBJ 7	0.40	0.80	0.7	−0.136	2
	1.50	0.20	0.05	$-\infty$	2
	0.40	0.82	0.20	−0.150	2

The design conditions and constraints are summarized in Table 1. The corresponding optimal shapes are designated as case GBJ 1 to case GBJ 7. The number of wing sections subject to design was equal to 2 (crank and tip).

As already mentioned, the optimization method is an iterative one. As a whole, the algorithm showed good convergence properties. The objective function convergence history is exemplified for case GBJ 1 in Fig. 2. Specifically, about 8–12 optimization steps were needed to converge the overall optimization process. For all the considered cases, the population size was equal to 200, the number of design variables was equal to 38, and the average number of generations run per GA optimization search was equal to 2000. The number of Navier–Stokes computations per optimization step was equal to 47 (38 for the database construction stage and 9 for the verification stage). The computations were performed on a computer cluster with 316 IBM BladeCenter processors. In terms of wall-clock time consumption, one single-point optimization requires (on the preceding cluster) about 15–18 h.

The first five cases deal with one-point optimization at two design points: $C_L = 0.52$ ($M = 0.75$) and $C_L = 0.40$ ($M = 0.80$) with different constraints placed upon the solution. The last two cases are related to multipoint optimization.

The original generic wing–body configuration possesses a moderate shock at $C_L = 0.52$ ($M = 0.75$). The corresponding pressure distribution is presented in Fig. 3. It is clearly seen that the shock covers most of the wing span, being especially strong in the vicinity of the crank. In terms of drag, the shock leads to a relatively high total drag value of the initial configuration: $C_D = 317.5$ aerodynamic counts.

The performed one-point optimization allowed us to essentially reduce the drag. Specifically, with no constraint placed upon the pitching moment (case GBJ 1), the total drag amounts to 304.1 counts. Though the maximum thickness of wing sections remained unchanged, the wing loading for the optimal geometry was

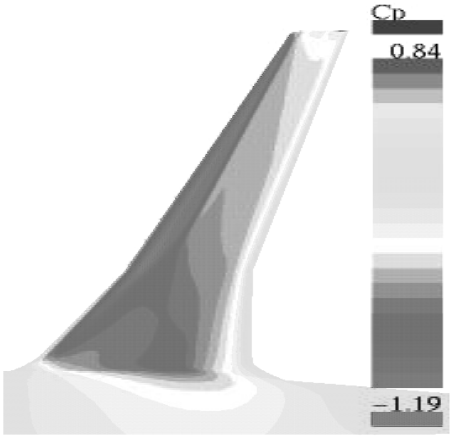

Fig. 3 Original generic business jet wing–body; pressure distribution on the upper surface of the wing at $M = 0.75$ and $C_L = 0.52$.

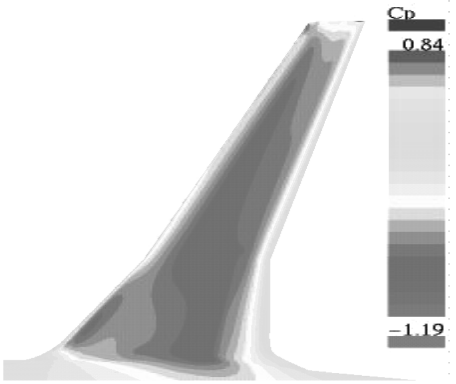

Fig. 4 Optimized generic business jet wing–body for case GBJ 1. Pressure distribution on the upper surface of the wing at $M = 0.75$ and $C_L = 0.52$.

strongly redistributed, compared with the original one. As seen from Fig. 4, the resulted pressure distribution is virtually shockless.

The drag reduction due to optimization is not pointwise. In terms of lift/drag curves, this gain is preserved in a wide range of C_L values. Moreover, as seen from Fig. 5, the drag reduction is only higher at higher lift coefficients.

The second considered design point possesses a higher freestream Mach number and a lower C_L value: $M = 0.80$ and $C_L = 0.40$. This combination of flight conditions leads to a significant change in the shock pattern. In particular, as can be assessed from the corresponding pressure distributions in Figs. 6 and 7, the original configuration is characterized by a λ-like spanwise shock development. At these conditions, the original configuration drag value is equal to $C_D = 292.0$ aerodynamic counts.

The performed unconstrained (with respect to C_M) one-point optimizations (case GBJ 2 and case GBJ 3) allowed us to reduce the drag to 275.3 and 275.9 counts, respectively. As seen from Table 1, in case GBJ 3, an additional constraint (compared with case GBJ 2) was imposed on local wing thickness at specified points (beam constraints).

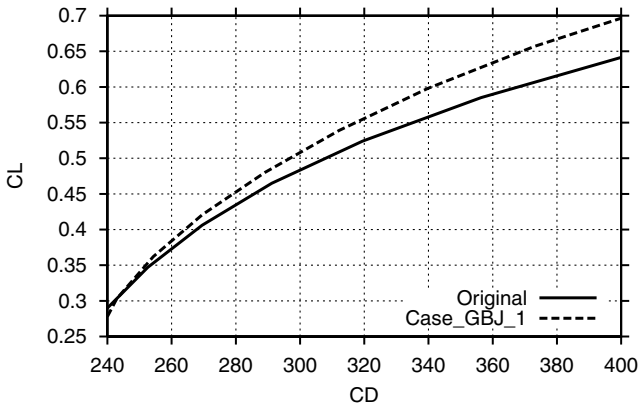

Fig. 5 Generic business jet wing–body; drag polars at $M = 0.75$; optimized configuration vs the original one.

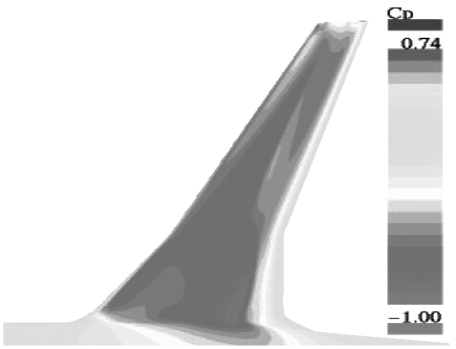

Fig. 6 Original generic business jet wing–body; pressure distribution on the upper surface of the wing at $M = 0.80$ and $C_L = 0.40$.

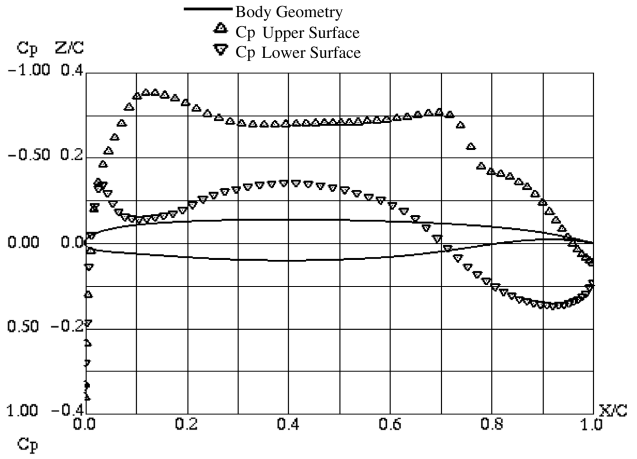

Fig. 7 Original generic business jet wing–body; $M = 0.80$ and $C_L = 0.40$; chordwise pressure distribution at $2y/b = 0.44$.

The corresponding pressure distributions are depicted in Figs. 8–10. The analysis of these pictures allowed us to conclude that the achieved drag reduction may be attributed to a significant decrease in the shock strength.

As already mentioned, the change in design conditions (case GBJ 1 vs case GBJ 2), yielded an essential change in the

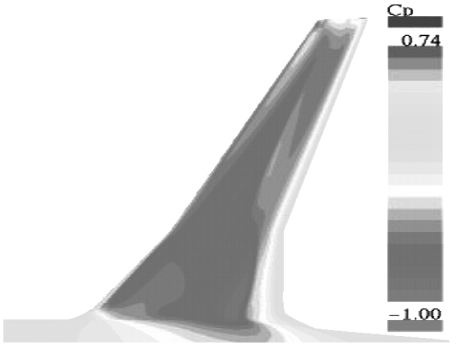

Fig. 8 Optimized generic business jet wing–body for case GBJ 2; pressure distribution on the upper surface of the wing at $M = 0.80$ and $C_L = 0.40$.

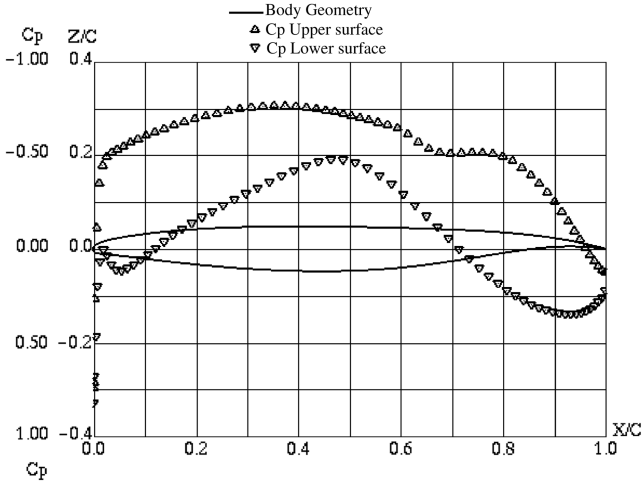

Fig. 9 Optimized generic business jet wing–body for case GBJ 2; $M = 0.80$ and $C_L = 0.40$; chordwise pressure distribution at $2y/b = 0.44$.

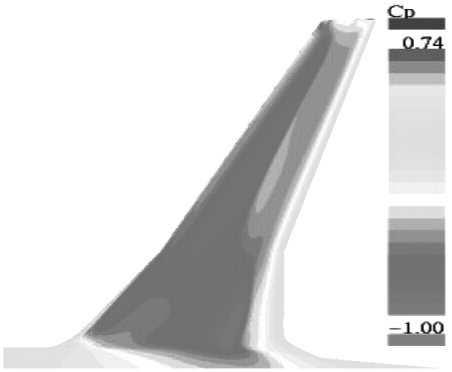

Fig. 10 Optimized generic business jet wing–body for case GBJ 3; pressure distribution on the upper surface of the wing at $M = 0.80$ and $C_L = 0.40$.

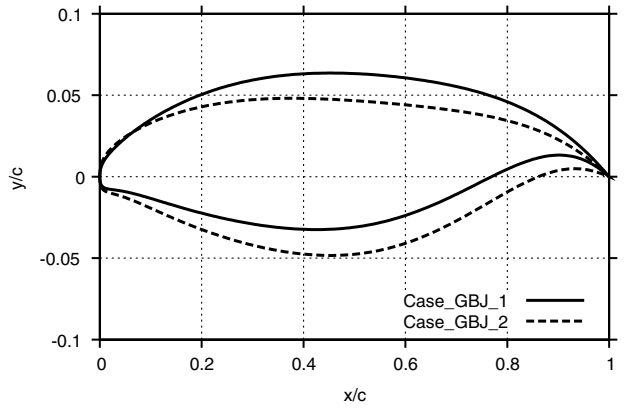

Fig. 11 Optimization of the generic business jet; crank section for case GBJ 1 vs case GBJ 2.

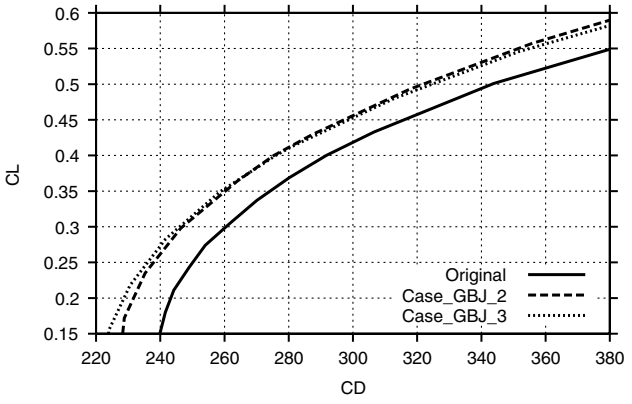

Fig. 12 Generic business jet wing–body; drag polars at $M = 0.80$; optimized configurations vs the original.

flow over the original configuration. In turn, this produced markedly different optimized wing shapes (see Fig. 11) corresponding to these flight conditions.

Off-design behavior of optimized configurations may be studied through lift/drag polars. These are presented in Fig. 12, in which the corresponding curves at $M = 0.80$ are compared with the original polar, thus illustrating the influence of the beam constraints on the results of optimization.

It can be concluded that the preceding local gains are preserved in a wide range of lift coefficient values from $C_L = 0.15$ to above 0.6. Additionally, we should note that the two optimized curves are close to one another, especially in a large vicinity of the design C_L. At the same time, in terms of shape, the difference between these optimization cases is significant for the both the crank and tip wing sections (see Figs. 13 and 14).

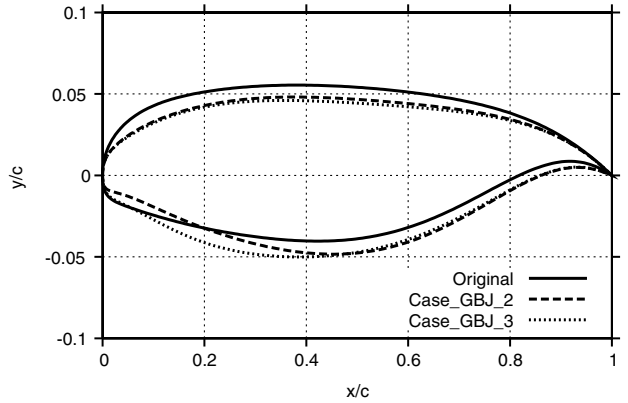

Fig. 13 Optimization of the generic business jet; crank section for case GBJ 2 and case GBJ 3 vs the initial geometry.

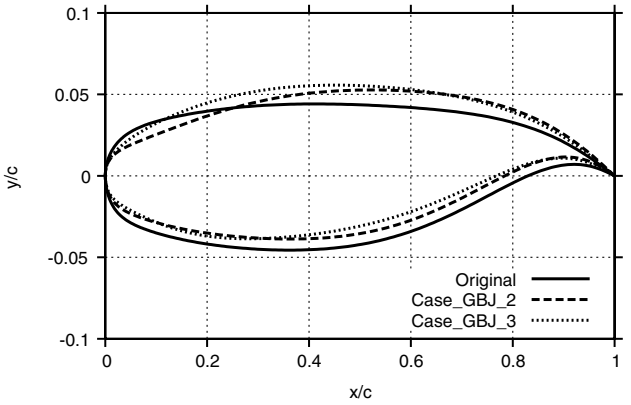

Fig. 14 Optimization of the generic business jet; tip section for case GBJ 2 and case GBJ 3 vs initial geometry.

Alongside the unconstrained pitching moment optimizations, the optimizations with constraint on C_M^* were performed. In case GBJ 4 and case GBJ 5, the value of C_M^* was kept to the original level ($C_M^* = -0.136$). These two cases differ in the presence of beam constraints, which were only imposed in case GBJ 5.

Let us compare the optimizations of case GBJ 2 and case GBJ 3 vs case GBJ 4 and case GBJ 5. As a whole, the penalty due to the imposition of pitching moment constraint was practically negligible: $C_D = 275.7$ counts for case GBJ 4 (about 0.4 counts higher with respect to case GBJ 2) and $C_D = 276.1$ counts for case GBJ 5 (0.2 counts higher than with case GBJ 3).

The comparison of the corresponding pressure distributions (Figs. 15–17) shows that the inclusion of the preceding constraint

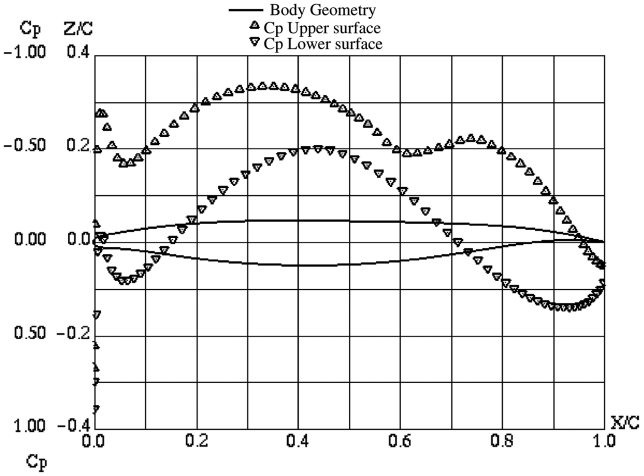

Fig. 15 Optimized generic business jet wing–body for case GBJ 4; $M = 0.80$ and $C_L = 0.40$; chordwise pressure distribution at $2y/b = 0.44$.

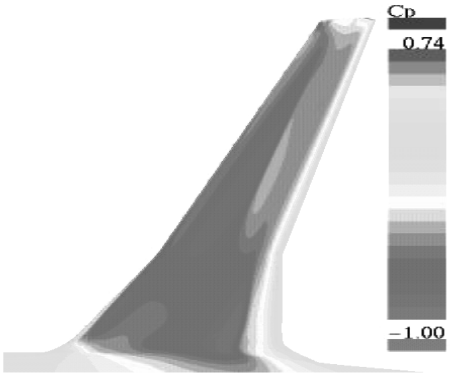

Fig. 16 Optimized generic business jet wing–body for case GBJ 5; pressure distribution on the upper surface of the wing at $M = 0.80$ and $C_L = 0.40$.

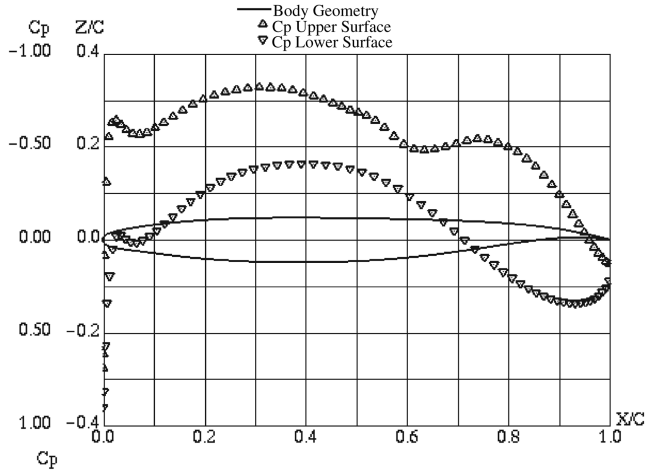

Fig. 17 Optimized generic business jet wing–body for case GBJ 5; $M = 0.80$ and $C_L = 0.40$; chordwise pressure distribution at $2y/b = 0.44$.

resulted (as aerodynamically expected) in a higher loading of the leading-edge area of the wing, especially of its inboard part.

In terms of shape modification, the influence of the optimization parameters on the specific form of the tip wing section can be assessed from Fig. 18. It is interesting that the optimization algorithm (operating in the automatic mode) employs very different ways to achieve its goals for different sets of constraints (especially in the wing leading-edge region). Specifically, for case GBJ 4, a solution with the significant leading-edge droop was found, whereas for case GBJ 5, the droop is only weakly indicated and the wing possesses a higher volume.

From the both theoretical and practical view points, it is interesting to know whether the optimal shapes are unique. The preceding comparison of optimal shapes provides a clarifying example on the subject. We see that very close values of total drag may correspond to significantly different wing geometries.

The last two cases (GBJ 6 and GBJ 7) are related to two- and three-point optimizations that take into account the full set of constraints. In case GBJ 6, cruise and takeoff conditions were targeted, whereas in case GBJ 7, the additional design point at a higher $M = 0.82$ was added.

The results were as follows. At the main design point ($C_L = 0.40$ and $M = 0.80$), the total drag value for case GBJ 6 was equal to 276.1 counts, compared with 275.6 counts for case GBJ 7. At the same time, at the high-Mach secondary design point, the three-point optimization achieved, as expected, a higher drag reduction: $C_D =$ 304.0 counts (case GBJ 6) vs $C_D = 295.0$ counts (case GBJ 7) (compared with the original 321.5 counts).

The resulting pressure distributions for the optimal generic business jet configurations are depicted in Figs. 19–21.

The influence of the multipoint design on the optimized shapes vs one-point optimization may be assessed from Fig. 22. It can be observed that the requirements coming from the takeoff design point resulted in a significant reshape of the outboard wing and in a moderate change in the form of the leading and trailing edges close to the crank section.

The comparison of the corresponding drag polars at the design Mach value is given in Fig. 23. The observed advantage of the three-point optimization, starting from $C_L = 0.4$, which increases at higher lift values, arises from the influence of the high-Mach secondary design point.

In conclusion, let us present the results of comparison between two- and three-point optimizations (case GBJ 6 vs case GBJ 7). In

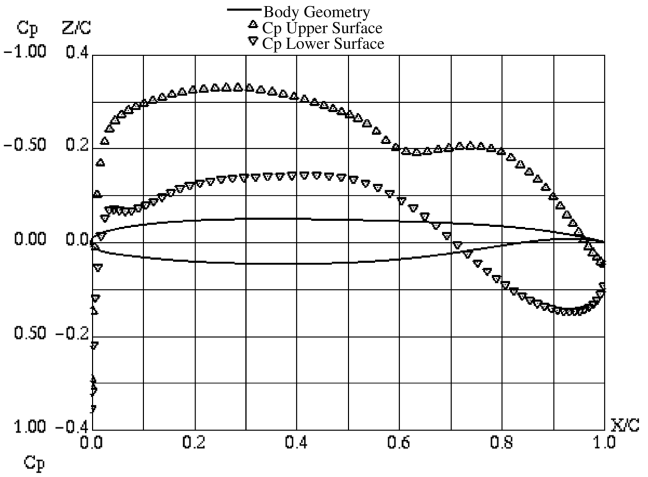

Fig. 19 Optimized generic business jet wing–body for case GBJ 6; $M = 0.80$ and $C_L = 0.40$; chordwise pressure distribution at $2y/b = 0.44$.

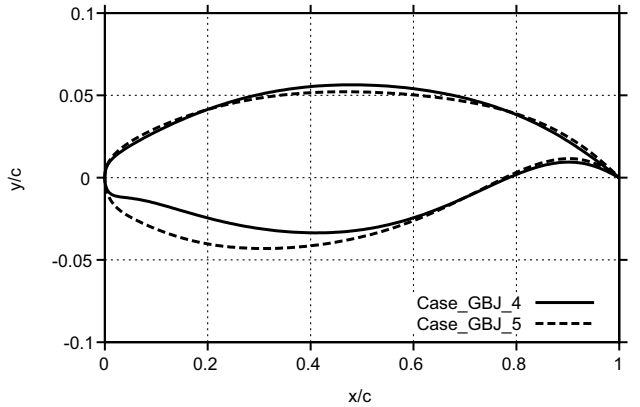

Fig. 18 Optimization of the generic business jet; tip section for case GBJ 4 vs case GBJ 5.

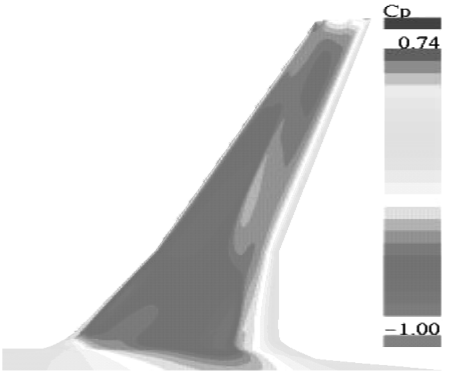

Fig. 20 Optimized generic business jet wing–body for case GBJ 7; pressure distribution on the upper surface of the wing at $M = 0.80$ and $C_L = 0.40$.

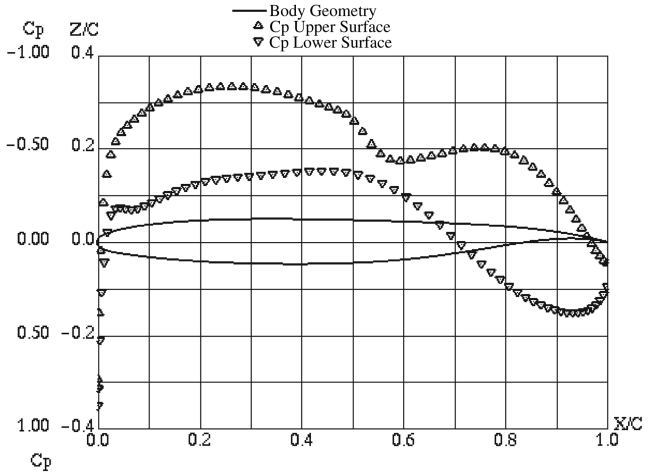

Fig. 21 Optimized generic business jet wing–body for case GBJ 7; $C_L = 0.40$; chordwise pressure distribution at $2y/b = 0.44$.

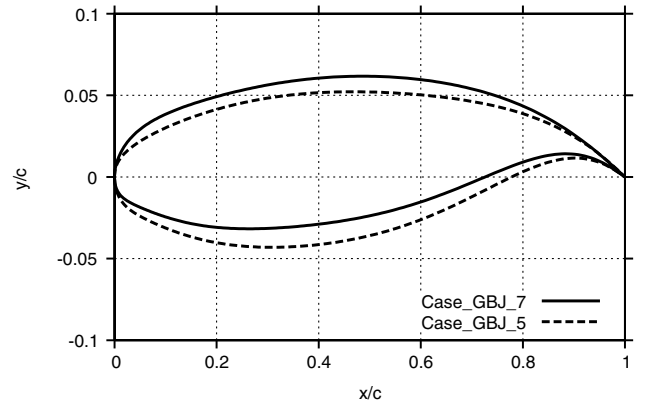

Fig. 22 Optimization of the generic business jet; tip section for case GBJ 5 vs case GBJ 7.

terms of shape, the influence of the third design point at a higher-than-cruise Mach value mainly resulted in a moderate reshaping of the wing tip airfoil (Fig. 24).

In terms of lift/drag polars (see Figs. 25 and 26), a slight advantage of case GBJ 7 noted at the main design Mach freestream value essentially increases at $M = 0.82$.

Another practically important off-design characteristics is Mach drag rise at a fixed lift coefficient. The corresponding data may be found in Fig. 27, in which Mach drag rise curves at $C_L = 0.4$ for one-point (case GBJ 2) and three-point (case GBJ 7) optimizations are presented. In both cases, the optimization succeeded to shift the Mach drag divergence point to at least the main Mach design value,

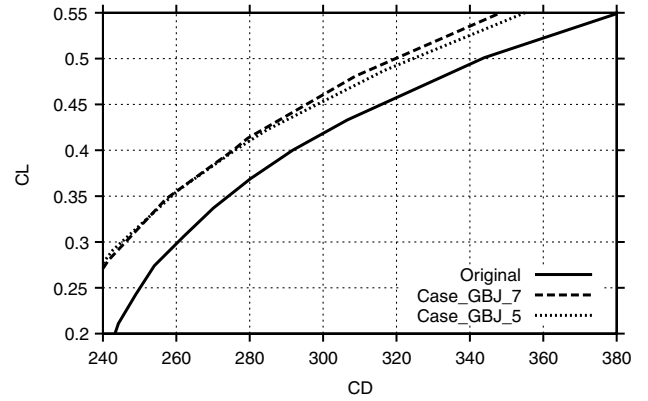

Fig. 23 Generic business jet wing–body; drag polars at $M = 0.80$; optimized configurations for case GBJ_5 and case GBJ_7 vs the original.

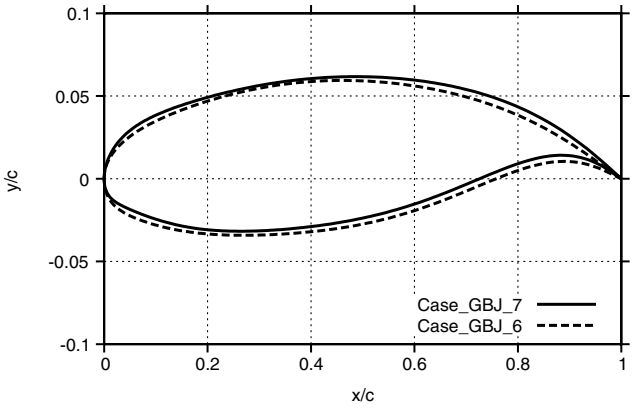

Fig. 24 Optimization of the generic business jet; tip section for case GBJ 6 vs case GBJ 7.

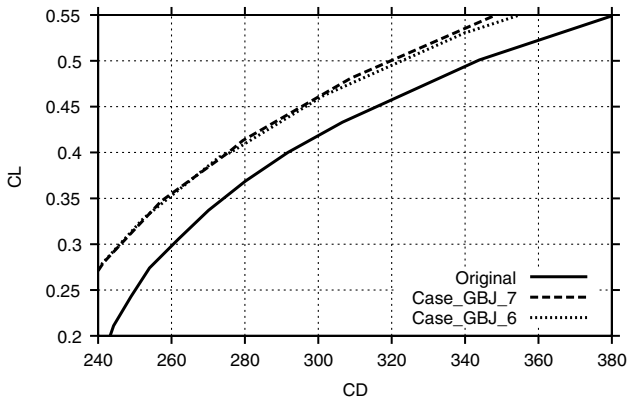

Fig. 25 Generic business jet wing–body; drag polars at $M = 0.80$; optimized configurations for case GBJ 6 and case GBJ 7 vs the original.

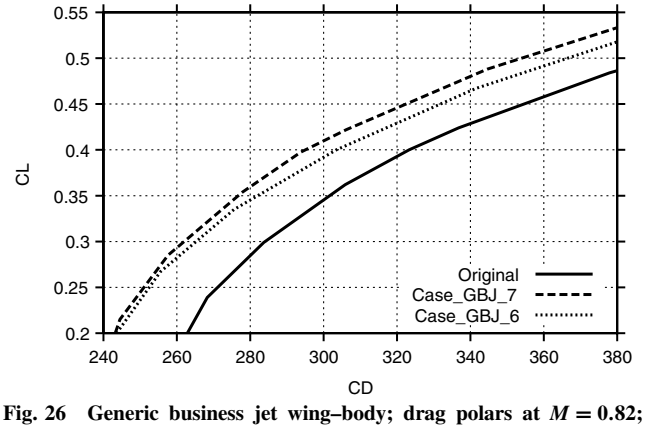

Fig. 26 Generic business jet wing–body; drag polars at $M = 0.82$; optimized configurations for case GBJ 6 and case GBJ 7 vs the original.

especially in the multipoint optimization. Specifically, based on the definition of the Mach drag divergence point as the Mach value for which $\partial C_D/\partial M = 0.1$, the corresponding M_{DD} value for the original configuration is equal to 0.795, whereas for the three-point optimization, $M_{\mathrm{DD}} = 0.815$. Additionally, the subsonic drag level (apparently due to reduction of form drag) is also decreased.

As mentioned in the problem statement, an additional off-design requirement is to preserve $C_L^{\max}$ value at the takeoff conditions. It may be seen from Fig. 28 that one-point optimizations do not necessarily support this property, whereas the multipoint optimizations (in which the corresponding design point is included) allow us to keep $C_L^{\max}$ to the required original level. The corresponding wing tip airfoil sections for case GBJ 2 and case GBJ 7 are, respectively, presented in Figs. 14 and 24.

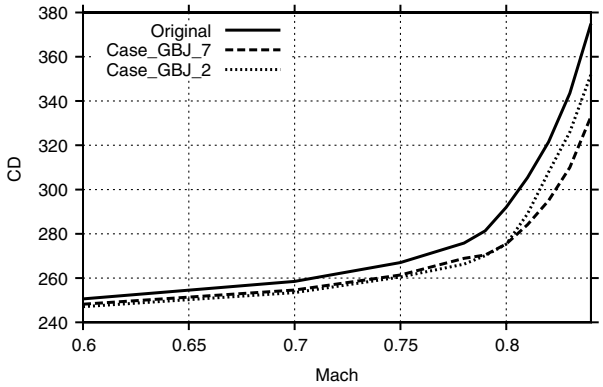

Fig. 27 Generic business jet wing–body; Mach drag divergence at $C_L = 0.40$; optimized configurations vs the original.

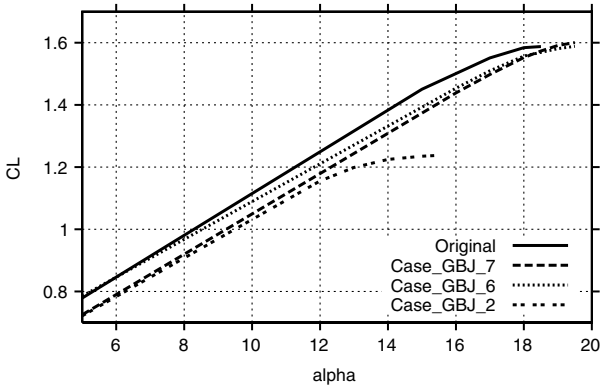

Fig. 28 Generic business jet wing–body; lift vs angle-of-attack curves at $M = 0.20$; optimized configurations vs the original.

V. Conclusions

The multiconstrained optimization of a generic business jet aircraft was considered. It may be concluded that the multipoint optimization allows for design of feasible aerodynamic shapes that possess a low drag at cruise conditions, satisfy a large number of geometrical and aerodynamic constraints, and offer good off-design performance in markedly different flight conditions such as takeoff conditions and high-Mach zone.

References

[1] Tennekes, H., *The Simple Science of Flight: From Insects to Jumbo Jets*, MIT Press, Cambridge, MA, 1997.

[2] Jameson, A., Martinelli, L., and Vassberg, J., "Using Computational Fluid Dynamics for Aerodynamics—a Critical Assessment," ICAS 2002, Edinburgh, Scotland, U.K., International Council of the Aeronautical Sciences, Paper 2002-1.10.1, 2002.

[3] Bauer, F., Garabedian, P., Korn, D., and Jameson, A., *Supercritical Wing Sections 2*, Springer–Verlag, New York, 1975.

[4] Hicks, R. M., and Henne, P. A., "Wing Design by Numerical Optimization," *Journal of Aircraft*, Vol. 15, No. 4, 1978, pp. 407–412.

[5] Jameson, A., "Aerodynamic Design via Control Theory," *Journal of Scientific Computing*, Vol. 3, No. 3, 1988, pp. 233–260. doi:10.1007/BF01061285

[6] "Optimum Design Methods for Aerodynamics," AGARD Rept. R-803, 1994.

[7] Jameson, A., "Optimum Aerodynamic Design Using Control Theory," *CFD Review*, Wiley, New York, 1995, pp. 495–528.

[8] Vicini, A., and Quagliarella, D., "Inverse and Direct Airfoil Design Using a Multiobjective Genetic Algorithm," *AIAA Journal*, Vol. 35, No. 9, 1997, pp. 1499–1505.

[9] Obayashi, S., Yamaguchi, Y., and Nakamura, T., "Multiobjective Genetic Algorithm for Multidisciplinary Design of Transonic Wing Planform," *Journal of Aircraft*, Vol. 34, No. 5, 1997, pp. 690–693.

[10] Hajela, P., "Nongradient Methods in Multidisciplinary Design Optimization—Status and Potential," *Journal of Aircraft*, Vol. 36, No. 1, 1999, pp. 255–265.

[11] Mohammadi, B., and Pironneau, O., *Applied Shape Optimization for Fluids*, Oxford Univ. Press, Oxford, 2001.

[12] Nadarajah, S. K., and Jameson, A., "Studies of the Continuous and Discrete Adjoint Approaches to Viscous Automatic Aerodynamic Shape Optimization," AIAA Paper 2001-2530, 2001.

[13] Vassberg, J. C., and Gregg, R. D., "Overview of Aerodynamic Design for Transport Aircraft," *Proceedings of the First MIT Conference on Computational Fluid and Solid Mechanics*, MIT Press, Cambridge, MA, June 2001.

[14] Epstein, B., and Peigin, S., "Constrained Aerodynamic Optimization of 3D Wings Driven by Navier–Stokes Computations," *AIAA Journal*, Vol. 43, No. 9, 2005, pp. 1946–1957.

[15] Epstein, B., Rubin, T., and Seror, S., "Accurate Multiblock Navier–Stokes Solver for Complex Aerodynamic Configurations," *AIAA Journal*, Vol. 41, No. 4, 2003, pp. 582–594.

[16] Shu, C.-W., and Osher, S., "Efficient Implementation of Essentially Non-Oscillatory Shock-Capturing Schemes," *Journal of Computational Physics*, Vol. 83, No. 1, 1989, pp. 32–78. doi:10.1016/0021-9991(89)90222-2

[17] Seror, S., Rubin, T., Peigin, S., and Epstein, B., "Implementation and Validation of the Spalart-Allmaras Turbulence Model for a Parallel CFD Code," *Journal of Aircraft*, Vol. 42, No. 1, 2005, pp. 179–188.

[18] Epstein, B., and Peigin, S., "Robust Hybrid Approach to Multiobjective Constrained Optimization in Aerodynamics," *AIAA Journal*, Vol. 42, No. 8, 2004, pp. 1572–1581.

[19] Michalewicz, Z., *Genetic Algorithms + Data Structures = Evolution Programs*, Springer–Verlag, New York, 1996.

[20] Sefrioui, M., Periaux, J., and Ganascia, J.-G., *Fast Convergence Thanks to Diversity Proceedings of the 5th Annual Conference on Evolutionary Programming*, MIT Press, Cambridge MA, 1996, pp. 321–335.

[21] Peigin, S., and Epstein, B., "Robust Handling of Non-Linear Constraints for GA Optimization of Aerodynamic Shapes," *International Journal for Numerical Methods in Fluids*, Vol. 45, No. 11, 2004, pp. 1339–1362. doi:10.1002/fld.747

[22] Peigin, S., and Epstein, B., "Embedded Parallelization Approach for Optimization in Aerodynamic Design," *Journal of Supercomputing*, Vol. 29, No. 3, 2004, pp. 243–263. doi:10.1023/B:SUPE.0000032780.68664.1b

[23] Peigin, S., Epstein, B., Rubin, T., and Seror, S., "Parallel Large Scale High Accuracy Navier–Stokes Computations on Distributed Memory Clusters," *The Journal of Supercomputing*, Vol. 27, No. 1, 2004, pp. 49–68. doi:10.1023/A:1026246805774

[24] Epstein, B., Averbuch, A., and Yavneh, I., "An Accurate ENO Driven Multigrid Method Applied to 3D Turbulent Transonic Flows," *Journal of Computational Physics*, Vol. 168, No. 3, 2001, pp. 316–338. doi:10.1006/jcph.2001.6698

[25] Weinerfelt, P., "Gradient Based Optimization of ONERA M6 Wing," *INGENET Workshop*, Centro Italiano Ricerche Aerospaziali, Capua, Italy, Jan. 27–28 2000.

N. Alexandrov
Associate Editor